doi.org/10.36721/PJPS.2026.39.7.194.1

Polydopamine-coated hollow mesoporous silica nanoparticles loaded with lupeol regulates immune microenvironment in gastric cancer mice by down-regulating IL-10 through regulating NF-κb signaling

Huijun Zhang[1], Xinyan Wei[2]*, Jun Guo[3] and Jing Shu[3]

[1]Health Management Center, Gansu Provincial Hospital of Traditional Chinese Medicine, Lanzhou, Gansu, 730050, China

[2]Department of Rheumatic and Osteopathic Diseases II, Gansu Provincial Hospital of Traditional Chinese Medicine, Lanzhou, Gansu, 730050, China

[3]Diagnosis and Treatment Center for Spleen and Stomach Diseases, Gansu Provincial Hospital of Traditional Chinese Medicine, Lanzhou, Gansu, 730050, China

Abstract: **Background**: Modulating the immune microenvironment is a promising strategy against gastric cancer. **Objectives**: This study explored the mechanism of polydopamine-coated hollow mesoporous silica nanoparticles loaded with lupeol (Lupeol-PDA-HMSNs) in regulating the immune microenvironment via the NF-κB/IL-10 axis. **Methods**: Lupeol-PDA-HMSNs were synthesized and characterized. A gastric cancer mouse model was established and mice were randomly assigned to control, free Lupeol, PDA-HMSNs, or Lupeol-PDA-HMSNs groups. Tumor growth was monitored. Immune cell profiles and serum cytokines were assessed by ELISA and flow cytometry. Apoptosis-related proteins and NF-κB pathway markers were evaluated by RT-qPCR and Western blot. NF-κB p65 binding to the IL-10 promoter was examined by ChIP-qPCR. **Results**: Lupeol-PDA-HMSNs were successfully synthesized, exhibiting a uniform particle size of 24.85 ± 0.14 nm and a zeta potential of -21.8 mV. Compared to the NC group, Lupeol-PDA-HMSNs significantly inhibited tumor growth, showing superior efficacy to both free lupeol and the blank carrier ($P<0.05$). The treatment markedly reduced the proportion of Tregs, while enhancing the populations of CD3+CD4+ T cells and NK cells, as well as the CD4+/CD8+ ratio. Additionally, it up-regulated the expression of pro-apoptotic proteins Bax and Caspase-3, down-regulated the anti-apoptotic protein Bcl-2 and consequently promoted apoptosis. Furthermore, Lupeol-PDA-HMSNs suppressed the activity of the NF-κB pathway, leading to reduced expression of downstream inflammatory cytokines IL-6, IL-10 and TNF-α. ChIP-qPCR analysis confirmed that NF-κB p65 directly binds to the IL-10 promoter region (-1648 to -1638) and this binding was significantly attenuated by Lupeol-PDA-HMSNs treatment ($P<0.01$). **Conclusion**: Lupeol-PDA-HMSNs exert potent anti-tumor effects by promoting apoptosis and modulating the immune microenvironment through inhibition of the NF-κB/IL-10 pathway, highlighting their potential as a nanotherapeutic strategy for gastric cancer.

Keywords: Immune microenvironment; Lupeol; NF-kb signaling pathway; Polydopamine-coated hollow mesoporous silica nanoparticles

Submitted on 20-11-2025 – Revised on 09-02-2026 – Accepted on 23-02-2026

INTRODUCTION

The tumor immune microenvironment constitutes a complex network of interactions between immune cells, tumor cells and stromal components, critically influencing tumor progression and therapeutic response (Mao *et al*., 2021). In gastric cancer, an immunosuppressive milieu characterized by abundant regulatory T cells (Tregs) facilitates tumor immune evasion and limits treatment efficacy (Kumagai *et al*., 2022). Among the key regulators of this process, the transcription factor NF-κB plays a pivotal role by controlling the expression of multiple genes involved in inflammation and immune modulation. Activation of NF-κB signaling by various cytokines has been closely associated with tumor progression and therapy resistance (Xu *et al*., 2022). However, the precise mechanisms through which NF-κB regulates immune escape in gastric cancer remain incompletely understood.

**Corresponding author:* e-mail: 13993199903@163.com

Interleukin-10 (IL-10), an immunosuppressive cytokine, exhibits complex and context-dependent roles in cancer biology (Shiri *et al*., 2024). Elevated IL-10 levels in gastric cancer patients correlate with advanced disease stage and poor prognosis (Yu *et al*., 2024). Mechanistically, IL-10 promotes macrophage polarization toward an anti-inflammatory phenotype via STAT3 pathway activation, while upregulating SOCS3 to inhibit immune cell activation and attenuate antitumor responses (Yan *et al*., 2022). This cytokine further establishes immune tolerance within the gastric cancer microenvironment, impairing effective tumor recognition and elimination. Despite these insights, whether NF-κB signaling directly regulates IL-10 expression in gastric cancer remains to be experimentally validated.

Lupeol, a natural pentacyclic triterpenoid, has demonstrated promising anti-inflammatory and pro-apoptotic activities in preclinical studies (Ahmad *et al*.,

2022). Its anticancer effects are partly attributed to mitochondrial dysfunction induction through inhibition of respiratory chain complex I, leading to apoptosis activation (Park and Lee, 2025). However, clinical translation of lupeol is hindered by poor bioavailability and limited tumor targeting. Recent advances in nanomedicine offer potential solutions; polydopamine-coated hollow mesoporous silica nanoparticles (PDA-HMSNs) have emerged as effective drug carriers that protect payloads from degradation while enabling controlled release and enhanced tumor accumulation (Jadidi *et al*., 2022). Whether lupeol-loaded PDA-HMSNs (Lupeol-PDA-HMSNs) can modulate the gastric cancer immune microenvironment through NF-κB/IL-10 axis regulation represents an unexplored therapeutic opportunity.

Therefore, this study aimed to investigate the antitumor efficacy and immunomodulatory mechanisms of Lupeol-PDA-HMSNs in a murine gastric cancer model. We hypothesized that this nanoformulation would suppress tumor growth by inhibiting NF-κB signaling, downregulating IL-10 expression and consequently reprogramming the immunosuppressive microenvironment (Fig. 1). Our findings provide novel insights into nanocarrier-based immunotherapy and identify a potential strategy for gastric cancer treatment.

MATERIALS AND METHODS

Experimental materials

MFC gastric cancer cells were purchased from Shanghai Tongpai Biotechnology Co., Ltd. Lupeol (purity: ≥98%, batch number: 545-47-1, Shanghai Jizhi Biochemical); NF-κb inhibitor PDTC (purity: 99%, batch number: 5108-96-3, Beijing Biolabs); NF-κb activator Echinulin (purity: ≥98%, batch number: 1859-87-6, Wuhan Tianzhi Biology); monoclonal antibody (Wuhan Jinkairui); secondary antibody (Suzhou Boteron); ELISA kit (Shanghai Keaibo); Hematoxylin (Shanghai Kaiyin Chemical Industry); Eosin dye (Changsha Hanchen Biological).

The chemical structures of related materials are shown in Fig. 2.

Preparation and characterization of Lupeol-PDA-HMSNs

Synthesis of HMSNs

HMSNs were synthesized using a template-etching method. First, solid SiO_2 spheres were prepared by hydrolyzing tetraethyl orthosilicate (TEOS) in an ethanol/water/ammonia mixture (volume ratio 50:10:1) at 30°C for 6 h with continuous stirring. Subsequently, 100 mg of SiO_2 spheres were dispersed in 100 mL of ethanol/water solution (4:1, v/v), followed by addition of 0.5 g cetyltrimethylammonium bromide (CTAB) as a template. TEOS (2 mL) was added dropwise and the reaction proceeded at 30°C for 24 h. The resulting core-shell particles were calcined at 550°C for 5 h to remove CTAB. Finally, the silica core was etched with 2.0 M Na_2CO_3 solution at 80°C for 4 h to obtain HMSNs.

PDA coating

HMSNs (50 mg) were dispersed in 50 mL of Tris-HCl buffer (10 mM, pH 8.5) by sonication for 15 min. Dopamine hydrochloride (20 mg) was added and the mixture was stirred at room temperature for 24 h. The resulting polydopamine-coated nanoparticles (PDA-HMSNs) were collected by centrifugation (12,000 ×g, 15 min), washed three times with deionized water and freeze-dried.

Drug loading

PDA-HMSNs (20 mg) and lupeol (5 mg) were co-dissolved in 10 mL of absolute ethanol and stirred at 25°C for 24 h in the dark. The drug-loaded nanoparticles (Lupeol-PDA-HMSNs) were separated by centrifugation (12,000 ×g, 20 min) and washed twice with ethanol to remove unencapsulated drug. The drug loading capacity and encapsulation efficiency were determined by measuring the residual lupeol concentration in the supernatant at 210 nm using UV-vis spectroscopy. The loading capacity was calculated as (weight of loaded drug / total nanoparticle weight) × 100% and encapsulation efficiency as (weight of loaded drug / initial drug weight) × 100%.

Characterization of nanomaterials

Morphology was examined by transmission electron microscopy (TEM, Hitachi HT7700). Hydrodynamic diameter and zeta potential were measured by dynamic light scattering (DLS, Malvern Zetasizer Nano ZS). The *in-vitro* drug release profile was evaluated by incubating Lupeol-PDA-HMSNs (5 mg) in 10 mL phosphate-buffered saline (PBS) at pH 7.4, 6.8 and 5.0 under gentle shaking (100 rpm) at 37°C. At predetermined time intervals, samples were centrifuged and the supernatant was analyzed by UV-vis spectroscopy to determine the cumulative drug release.

Experimental method

Gastric cancer mouse model

Using female BALB/c mice aged 6-8 weeks and weighing 18-22 g (purchased from Shanghai Xipuer-Bikai Experimental Animal Co., Ltd.). MFC gastric cancer cells were resuspended in PBS at a density of 1×10^7 cells/mL. Each mouse was subcutaneously injected with 0.2 mL of the cell suspension (containing 2×10^6 cells) into the right axillary region. After inoculation, daily observations were conducted. Approximately 7 days later, when a distinct subcutaneous nodule was palpable and its diameter exceeded 5 mm, the modeling was considered successful. The experimental design and proposed mechanism of action of Lupeol-PDA-HMSNs are illustrated in figure 1.

Group intervention

The successfully modeled mice were randomly divided

into the following groups: NC group, PDA-HMSNs group, Lupeol group, Lupeol-PDA-HMSNs group, PDTC group, Echinulin group and Lupeol-PDA-HMSNs+PDTC group, with 6 mice in each group.The NC group received intraperitoneal injections of sterile normal saline (1 mL/100 g body weight). The PDA-HMSNs group received intraperitoneal injections of 5 mg/kg PDA-HMSNs. The Lupeol group received intraperitoneal injections of 5 mg/kg free lupeol. The Lupeol-PDA-HMSNs group received intraperitoneal injections of 5 mg/kg Lupeol-PDA-HMSNs. The PDTC group received intraperitoneal injections of 10 mg/kg PDTC. The Echinulin group received intraperitoneal injections of 5 mg/kg Echinulin. The Lupeol-PDA-HMSNs+PDTC group received combined intraperitoneal injections of Lupeol-PDA-HMSNs (5 mg/kg) and PDTC (10 mg/kg). All interventions were administered on the 11th and 14th days after modeling.

Tumor volume change detection

Tumor volumes were measured by B-mode ultrasound at 1, 5, 10 and 14 days after the intervention and the tumor volume (V) was recorded.

Tumor weight measurement

After 16 days of intervention, mice were sacrificed by cervical dislocation to collect cancer tissue for analyzing tumor mass. Tumor volume = length × width 2 × 0.5.

HE pathological observation

Paraffin-embedded gastric tissues were fixed, sectioned (5 μm) and stained with hematoxylin to observe the pathological changes.

Measurement of peripheral blood immune parameters

Blood was collected from the retro-orbital area of the mouse, centrifuged (3 000 r/min) for 5 min to obtain supernatant. According to the instructions of the ELISA kit, CD3+ CD4+, Treg, natural killer (NK) cells, IL-10 level and calculate CD4+/CD8+.

Flow cytometry was used to detect cell apoptosis

Single-cell suspensions were prepared from 100 mg of tumor tissue at a concentration of 1×10^7 cells/mL. A 100 μL aliquot of the cell suspension was taken and 5 μL of Annexin V-FITC and 5 μL of propidium iodide (PI) were added. The mixture was incubated at room temperature in the dark for 15 minutes before being analyzed using a BD FACSCanto II flow cytometer (Chen and Xie, 2018). The gating strategy was as follows: First, debris was excluded by gating on the FSC-A/SSC-A scatter plot (P1). Next, doublets were excluded by gating on the FSC-A/FSC-H scatter plot to obtain the single-cell population (P2). Finally, apoptosis was analyzed on the Annexin V-FITC/PI scatter plot. Cells were distinguished as viable, early apoptotic and late apoptotic/necrotic based on their Annexin V and PI fluorescence signals.

RT-PCR

Total RNA was extracted from the tissues using TRIzol reagent and its purity and concentration were measured. Then, 1 μg of RNA was taken for reverse transcription (PrimeScript RT kit) to obtain cDNA. Quantitative real-time PCR (qPCR) was performed using SYBR Green Master Mix on an ABI 7500 system with the following program: 95°C for 30 seconds, followed by 40 cycles of 95°C for 5 seconds and 60°C for 30 seconds. GAPDH was used as the internal reference gene and the relative expression levels of the target genes were calculated using the $2-\Delta\Delta Ct$ method (Livak and Schmittgen, 2001). The primer sequences are listed in table 1.

Western blot

Proteins were extracted from the tissues using RIPA lysis buffer and quantified by the BCA method. Then, 30 μg of protein per sample was loaded, separated by 10% SDS-PAGE electrophoresis and transferred onto a PVDF membrane. The membrane was blocked with 5% skim milk at room temperature for 1 hour, followed by incubation with primary antibodies (e.g., NF-κB p65, IL-10, Caspase-3) at 4°C overnight and subsequent incubation with secondary antibodies at room temperature for 1 hour. The protein bands were visualized using ECL and their gray values were analyzed with ImageJ software. GAPDH was used as the internal reference for normalization.

Dual-luciferase reporter gene assay

The downstream target gene of NF-κb was predicted by the Targetscan database, which was identified as IL-10 here and the IL-10 3UTR WT and MUT sequences were amplified, co-transfected with a negative control sequence and a dual-luciferase assay was performed based on the instructions (Chen *et al*., 2020).

Chromatin immunoprecipitation - quantitative polymerase chain reaction (ChIP-qPCR)

The experiment was performed using a ChIP kit (Millipore, #17-295). MFC cells were cross-linked with 1% formaldehyde for 10 minutes and the chromatin was fragmented by sonication to sizes ranging from 200 to 500 bp. Immunoprecipitation was carried out using either an NF-κB p65 antibody (CST, #8242) or normal rabbit IgG. The precipitated DNA was purified and quantitatively analyzed using a SYBR Green qPCR system. Primers were designed to target the region of the IL-10 promoter containing the predicted NF-κB binding site: Forward: 5'-GAGAGCTGCCTTTTGGGAAT-3'; Reverse: 5'-CTGGGCTGGAGTTCAGTGT-3'. The results were calculated as fold enrichment using the "% Input" method.

Statistical analysis

SPSS21.0 and GraphPad Prism 8.0. software processed data. Data are presented as mean±standard deviation (SD). Differences between groups were analyzed by one-way ANOVA followed by Tukey's post-hoc test using SPSS 21.0. $P<0.05$ was considered statistically significant.

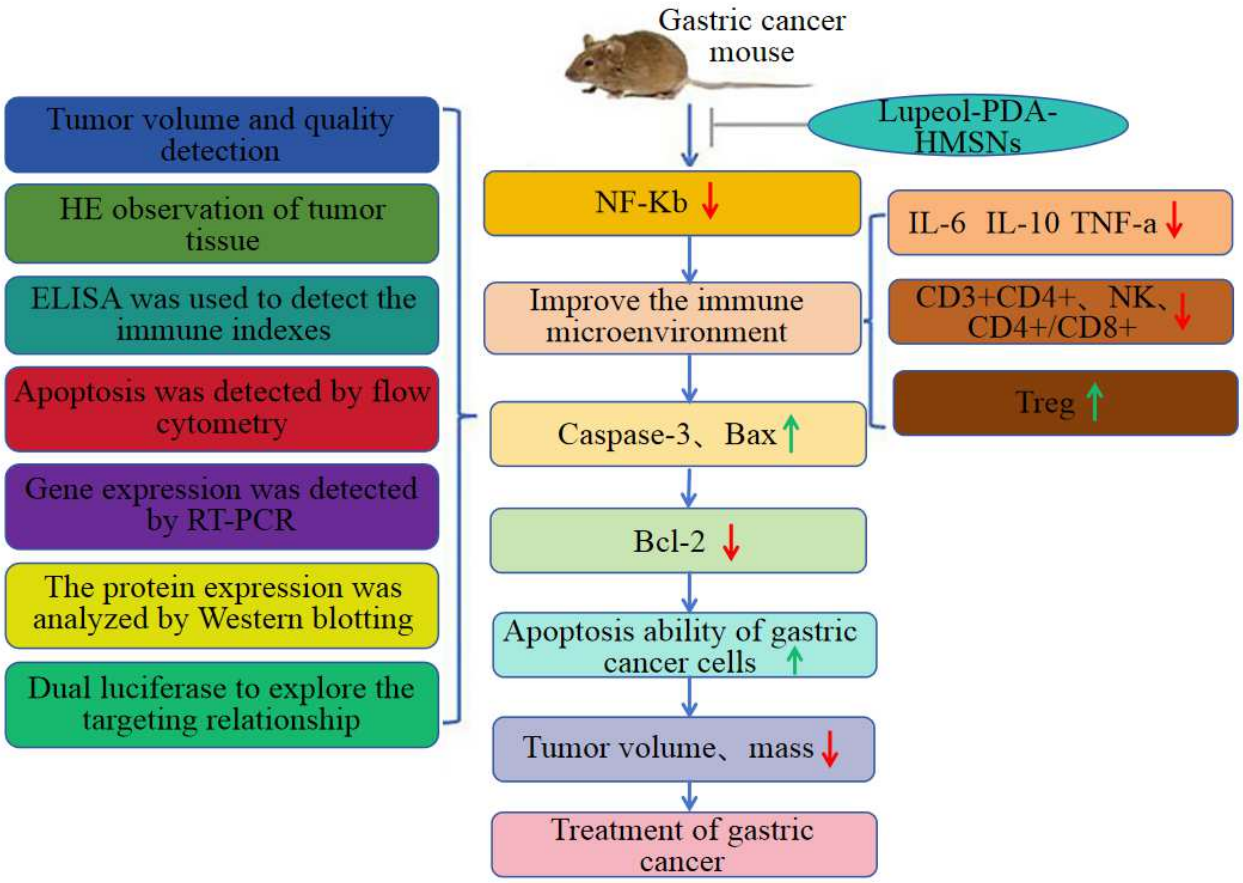

Fig. 1: Lupeol-PDA-HMSNs nanoparticles can down-regulate the expression of IL-10 by inhibiting NF-κB signaling activity, thereby improving the immune microenvironment of gastric cancer mice.

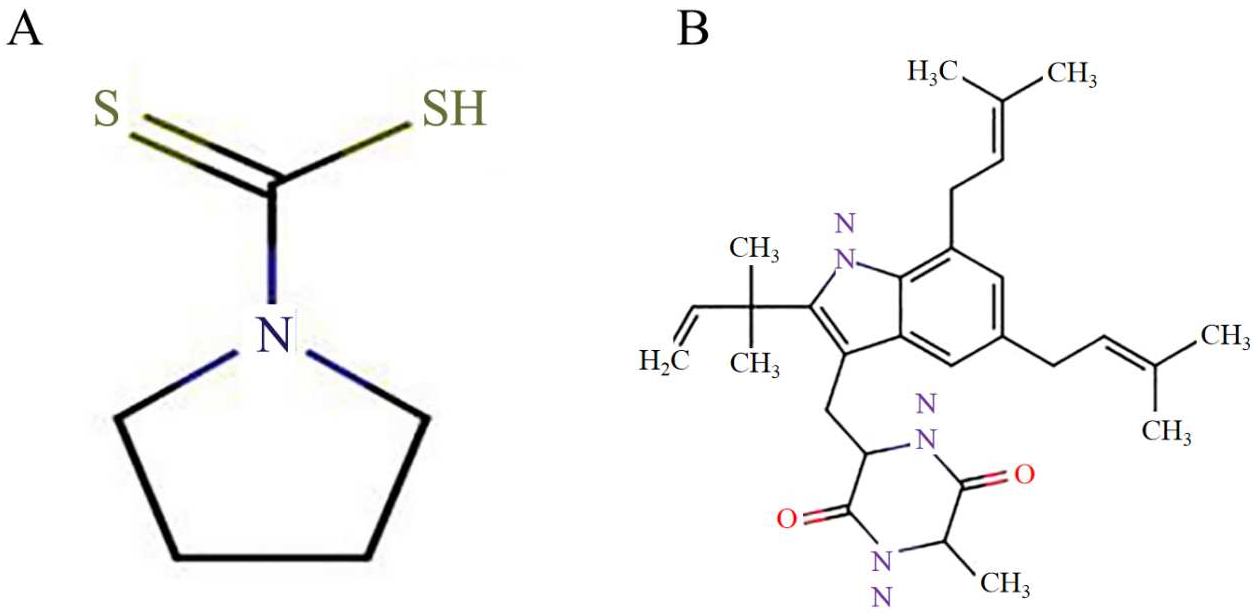

Fig. 2: Chemical structures of related materials.
(A) . The chemical structural formula of NF-κb inhibitor PDTC; (B). The chemical structural formula of NF-κb activator Echinulin.

Table 1: Real-time PCR primers and primer sequences.

Primer		Sequences
NF-kb	Forward primer	5'-GGAGAAGTGTCCAGGAAGTT-3'
	Reverse primer	5'-GTCCACTCTGCTGGAAAAAC-3'
IL-6	Forward primer	5'-TCATATCAGTTGCCTTCTCCTG-3'
	Reverse primer	5'-CAGAATTTCCATTTCCAACACTC-3'
IL-10	Forward primer	5'-CTGAAGACCTGCCACTTGCT-3'
	Reverse primer	5'-TGTTCATTTTCCGATTGCTG-3'
TNF-a	Forward primer	5'-GAATTCCAAGACACCTCACCC-3'
	Reverse primer	5'-TGGGAAGTTGGAGGGACTTT-3'
GAPDH	Forward primer	5'-AAAGGGTCATCATCTCCGCC-3'
	Reverse primer	5'-AGTGATGGCATGGACTGTGG-3'

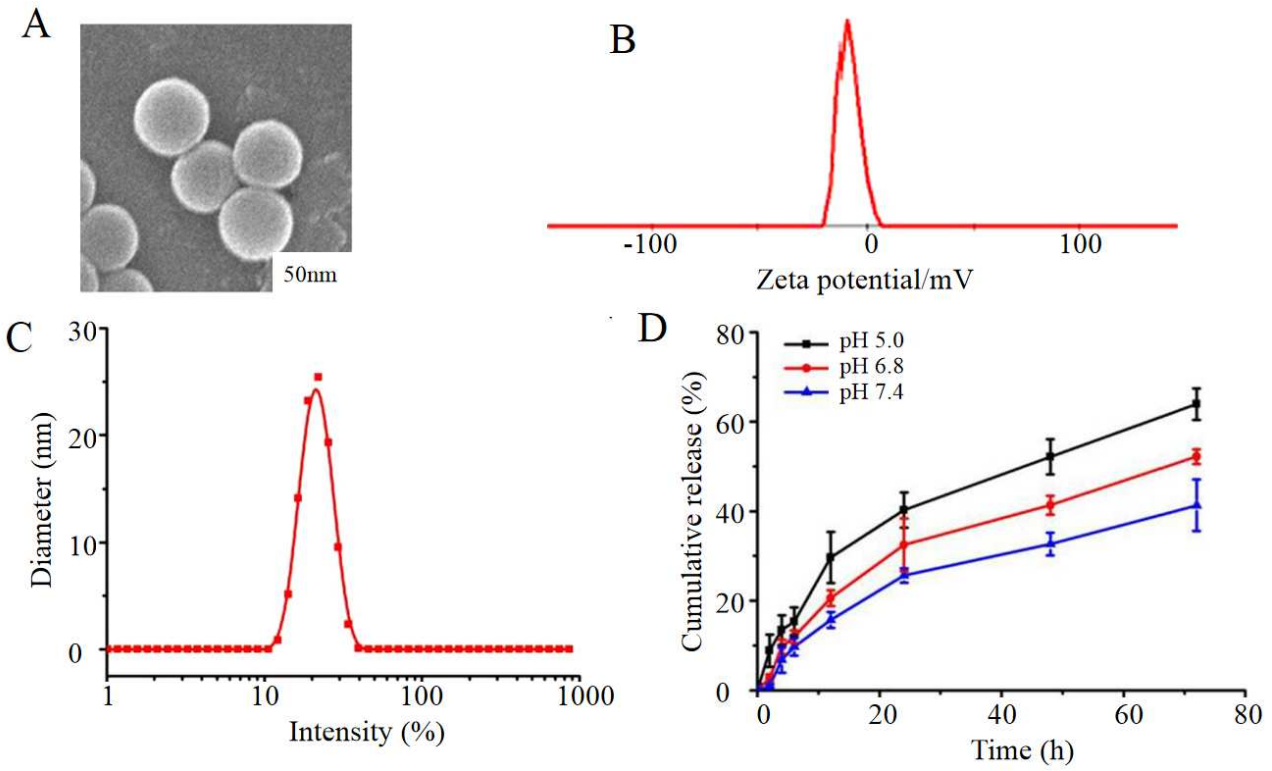

Fig. 3: Transmission electron microscope of Lupeol-PDA-HMSNs.
(A) TEM image of Lupeol-PDA-HMSNs; (B) Zeta potential distribution of Lupeol-PDA-HMSNs; (C) Particle size distribution of Lupeol-PDA-HMSNs; (D) *In-vitro* release profile of Lupeol-PDA-HMSNs.

RESULTS

Lupeol-PDA-HMSNs were successfully prepared

Lupeol-loaded polydopamine-coated hollow mesoporous silica nanoparticles (Lupeol-PDA-HMSNs) were successfully synthesized. Transmission electron microscopy (TEM) revealed uniform hollow spherical nanoparticles with an average diameter of 24.85 ± 0.14 nm and distinct mesoporous structure (Fig. 3A). After polydopamine coating, the nanoparticle surface appeared slightly rougher. Dynamic light scattering analysis showed a hydrodynamic size of 32.5 ± 1.2 nm and a zeta potential of -21.8 mV, indicating good colloidal stability (Fig. 3B). The drug loading capacity and encapsulation efficiency were calculated as 18.5 ± 1.2% and 86.3 ± 2.1%, respectively. *In-vitro* release studies demonstrated pH-responsive drug release, with significantly faster lupeol release observed at acidic pH (6.8 and 5.0) compared to physiological pH (7.4) (Fig. 3C).

Lupeol-PDA-HMSNs demonstrate significant tumor suppressive effects on gastric cancer, inhibit the expression of IL-10 and regulate immune microenvironment

During the model establishment and intervention period, no mouse deaths occurred and the modeling success rate reached 100%. A nodule diameter exceeding 5 mm was considered indicative of successful modeling. To elucidate

the therapeutic effect of lupeol-loaded polydopamine-coated hollow mesoporous silica nanoparticles (Lupeol-PDA-HMSNs) on mice with gastric cancer, tumor volumes were compared. Relative to the NC group, the PDA-HMSNs group showed no significant difference in tumor volume during the intervention period (P>0.05), indicating that the PDA-HMSNs carrier itself lacks direct antitumor activity. The tumor volume in the Lupeol group was significantly lower than that in the NC group (P<0.05), while the Lupeol-PDA-HMSNs group exhibited a further reduction in tumor volume compared to all other groups (P<0.05) (Fig. 4A). These results demonstrate that the nano-carrier system significantly enhances the therapeutic efficacy of lupeol.

A comparison of tumors after 16 days of intervention is shown in figure 4B. The results further revealed that the tumor mass in the lupeol-loaded polydopamine-coated hollow mesoporous silica nanoparticle (Lupeol-PDA-HMSNs) group was significantly lower compared to all other groups (P < 0.05), as illustrated in fig. 4C.

The results showed that the histopathological features of the NC group and the PDA-HMSNs group were similar, characterized by large, hyperchromatic tumor cell nuclei, active mitosis and prominent fibrous tissue proliferation. In the Lupeol group, nuclear atypia was slightly reduced, mitotic Fig.s decreased and the extent of fibrous hyperplasia was lower compared to the NC group. In contrast, the Lupeol-PDA-HMSNs group exhibited more regular nuclear morphology, reduced fibrous hyperplasia and significantly improved histopathological changes (P<0.05 compared to other groups) (Fig. 4D). These findings indicate that lupeol-loaded polydopamine-coated hollow mesoporous silica nanoparticles can inhibit gastric cancer progression to some extent.

Compared to the NC group, the expression level of IL-10 mRNA in peripheral blood showed no significant change in the PDA-HMSNs group (P>0.05). However, the Lupeol group significantly reduced IL-10 mRNA expression (P<0.05). Furthermore, intervention with lupeol-loaded polydopamine-coated hollow mesoporous silica nanoparticles led to an even more pronounced decrease in IL-10 mRNA levels (P<0.05) (Fig. 4E).

Further ELISA assays revealed that, compared to the NC group, the proportion of Treg cells in the PDA-HMSNs group showed no significant change (P > 0.05). Compared to the NC group, the Lupeol group showed significantly increased proportions of CD3+CD4+ T cells and NK cells, as well as the CD4+/CD8+ ratio. In contrast, the Lupeol-PDA-HMSNs group exhibited a significant increase in the proportions of CD3+CD4+ T cells and NK cells, along with a significantly elevated CD4+/CD8+ ratio, while the proportion of Treg cells was significantly reduced (P<0.05 compared to other groups) (Fig. 4F).

Lupeol-PDA-HMSNs can regulate immune microenvironment of gastric cancer mice by inhibiting NF-κb signaling pathway

Level of NF-κb in PDTC group was significantly decreased and the level in Echinulin group was increased (vs NC group, P<0.05), indicating that the interference of NF-κb signal activity was successful. At the same time, the study showed that the protein levels of NF-κb, IL-6, IL-10 and TNF-a in Lupeol-PDA-HMSNs group were significantly reduced (vs NC group, P<0.05), indicating that Lupeol-PDA-HMSNs can reduce the level of NF-κb and inhibit IL-6, IL-10 and TNF-a expression. After adding PDTC to the Lupeol-PDA-HMSNs group, the above protein levels decreased more significantly (P<0.05), indicating that Lupeol-PDA-HMSNs can play a synergistic role with PDTC to inhibit the expression of inflammatory factor proteins (Fig. 5A). Gene levels of NF-κb, IL-6, IL-10 and TNF-a also showed the same trend of change, the results are shown in figure 5B.

In addition, Echinulin significantly reduced the expression levels of CD3+CD4+, NK and CD4+/CD8+ and promote the expression of Treg and the PDTC group is the opposite (vs NC group, P<0.05). After adding Lupeol-PDA-HMSNs to the PDTC group, each immune index The change was more obvious (P<0.05) (Fig. 5C).

The gastric cancer tissues in NC group showed the characteristics of fibrosis, which showed the increase of collagen fibers in the gastric mucosa and submucosa. However, fibrosis degree in Lupeol-PDA-HMSNs group was significantly lower and the collagen fiber density in the gastric mucosa layer was relatively less (vs the NC group). After adding PDTC to Lupeol-PDA-HMSNs group, the fibrosis degree of gastric cancer tissue was lower (vs other several groups), the results are shown in figure 5D.

Lupeol-PDA-HMSNs can increase Caspase-3 and Bax proteins and reduce Bcl-2 expression (vs NC group, P<0.05), suggesting that Lupeol-PDA-HMSNs can promote gastric cancer tissue apoptosis to a certain extent. At the same time, after adding PDTC intervention, the changes in the levels of the above-mentioned apoptosis-related proteins were more obvious (P<0.05) (Fig. 5E).

To further investigate the effect of Lupeol-PDA-HMSNs on apoptosis in gastric cancer cells, we performed flow cytometric analysis (Fig. 5F). The gating strategy was as follows: debris was first excluded via FSC-A/SSC-A gating (P1 gate), followed by the exclusion of doublets via FSC-A/FSC-H gating (P2 gate). Apoptosis was then analyzed in the Annexin V-FITC/PI scatter plot. Statistical analysis showed that, compared to the NC group, the total apoptosis rate was significantly increased in the Lupeol group. In the Lupeol-PDA-HMSNs group, apoptosis was further enhanced, indicating that inhibition of the NF-κB pathway can synergistically promote tumor cell apoptosis.

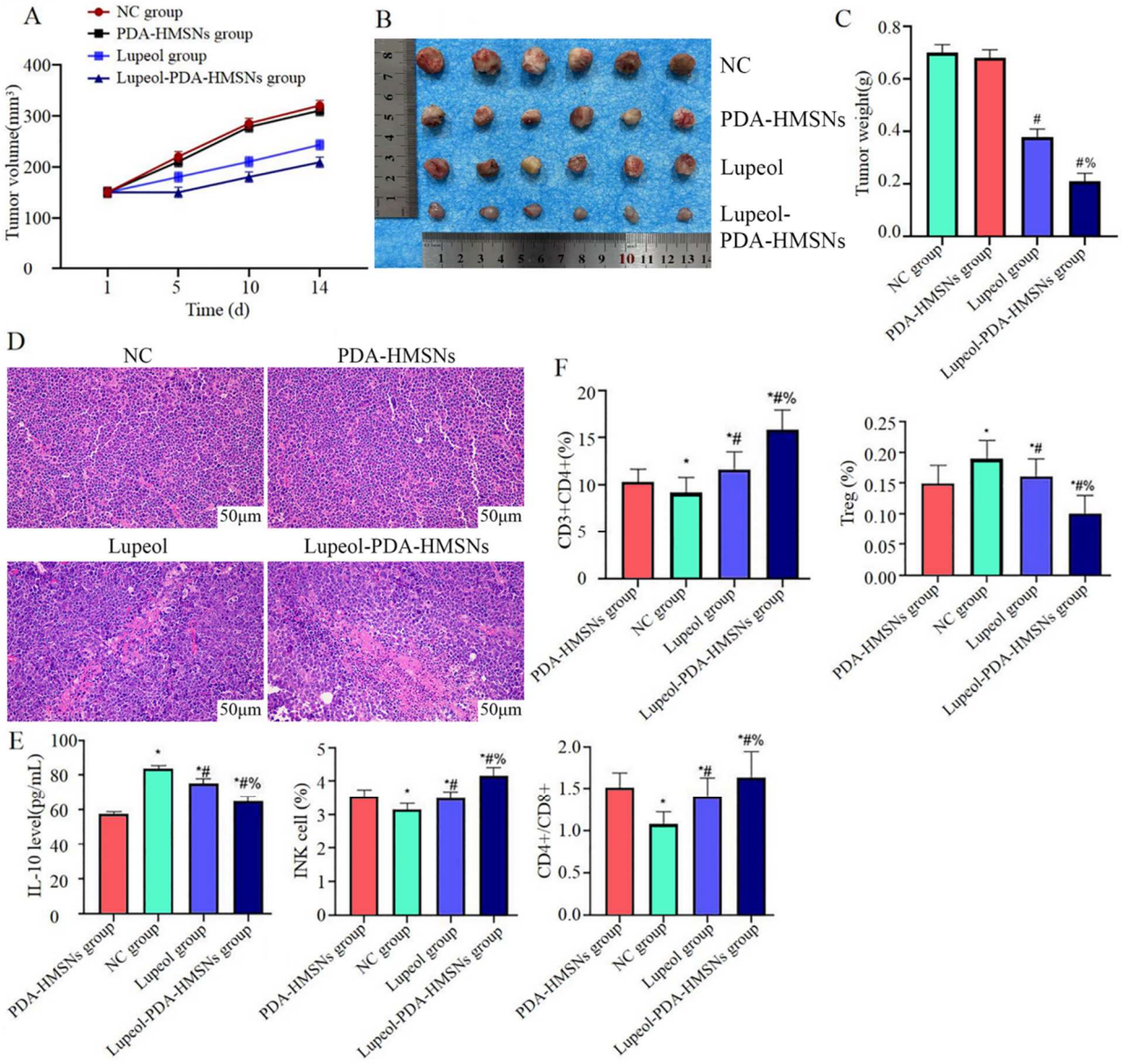

Fig. 4: Lupeol-PDA-HMSNs has a good tumor suppressor effect in gastric cancer, can inhibit the expression of IL-10 and regulate the immune microenvironment (n=6).
(A) Mouse tumor volume changes; (B) Mouse tumor size; (C) Mouse tumor mass histogram; (D) HE staining observation of gastric pathological changes, ×400; (E) qRT -PCR detection of tumor IL-10 mRNA expression; (F) ELISA test detection of peripheral blood immune indicators. Compared with control group, *P<0.05; compared with NC group, #P<0.05; compared with Lupeol group, %P<0.05.

NF-κB p65 directly binds to the IL-10 promoter region and is regulated by Lupeol-PDA-HMSNs

The ChIP-qPCR results (Fig. 6A) showed that in MFC gastric cancer cells, the NF-κB p65 subunit exhibited significant enrichment in the IL-10 promoter region (-1648 ~ -1638, containing the predicted κB site). The enrichment level was significantly higher than that in the nonspecific IgG control group (P<0.01), indicating that NF-κB p65 can directly bind to the IL-10 promoter under physiological conditions. To further investigate the effect of Lupeol-PDA-HMSNs on this binding process, MFC cells were treated with Lupeol, PDA-HMSNs, or Lupeol-PDA-HMSNs, followed by ChIP-qPCR analysis. As shown in Fig. 6B, compared to the control group, treatment with Lupeol-PDA-HMSNs significantly reduced the enrichment level of p65 in the IL-10 promoter region (P<0.01). In contrast, treatment with free Lupeol only caused a mild decrease (P<0.05), while PDA-HMSNs treatment had no significant effect (P>0.05). These findings indicate that NF-κB p65 can directly bind to the IL-10 promoter and positively regulate its transcription. Moreover, Lupeol-PDA-HMSNs effectively inhibit this binding process, thereby downregulating IL-10 expression at the transcriptional level.

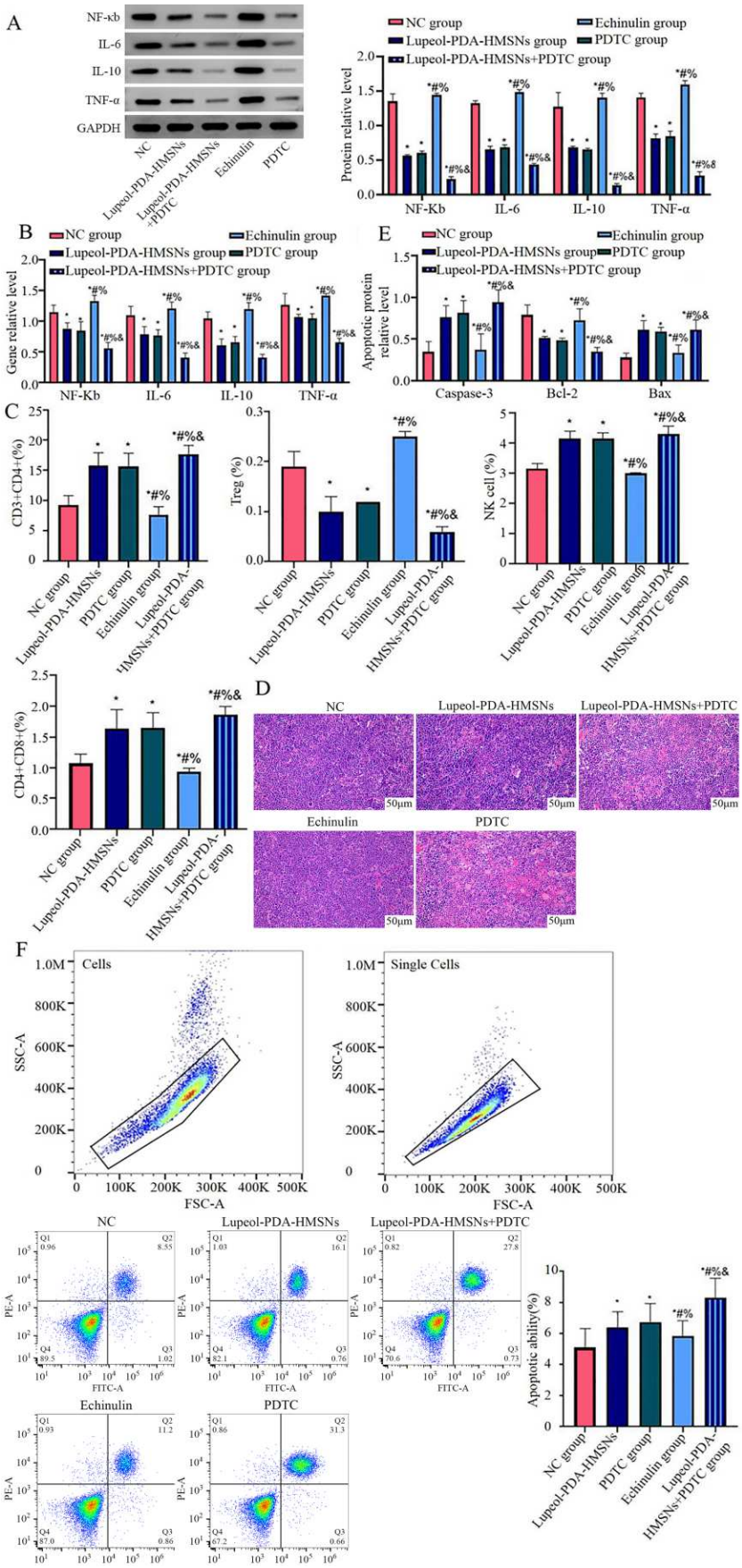

Fig. 5: Lupeol-PDA-HMSNs can regulate the immune microenvironment of gastric cancer mice by inhibiting the NF-κb signaling pathway (n=6). (A) Western blotting to observe the protein expression of NF-κb, IL-6, IL-10 and TNF-a, and the histogram shows the protein expression level; (B) qRT-PCR detection of NF-κb, IL-6, IL-10 and TNF-a mRNA expression; (C) ELISA detection of peripheral blood immune indicators; (D) HE staining to observe the pathological changes of gastric cancer; (E) The histogram shows the relative expression of apoptotic proteins; (F) The gating strategy is as follows: first, debris is excluded via FSC-A/SSC-A gating (P1 gate); then, doublets are excluded via FSC-A/FSC-H gating (P2 gate); finally, apoptosis is analyzed in the Annexin V-FITC/PI scatter plot. Compared with NC group, *P<0.05; compared with Lupeol-PDA-HMSNs group, #P<0.05; compared with PDTC group, %P<0.05; compared with Echinulin group, &P<0.05.

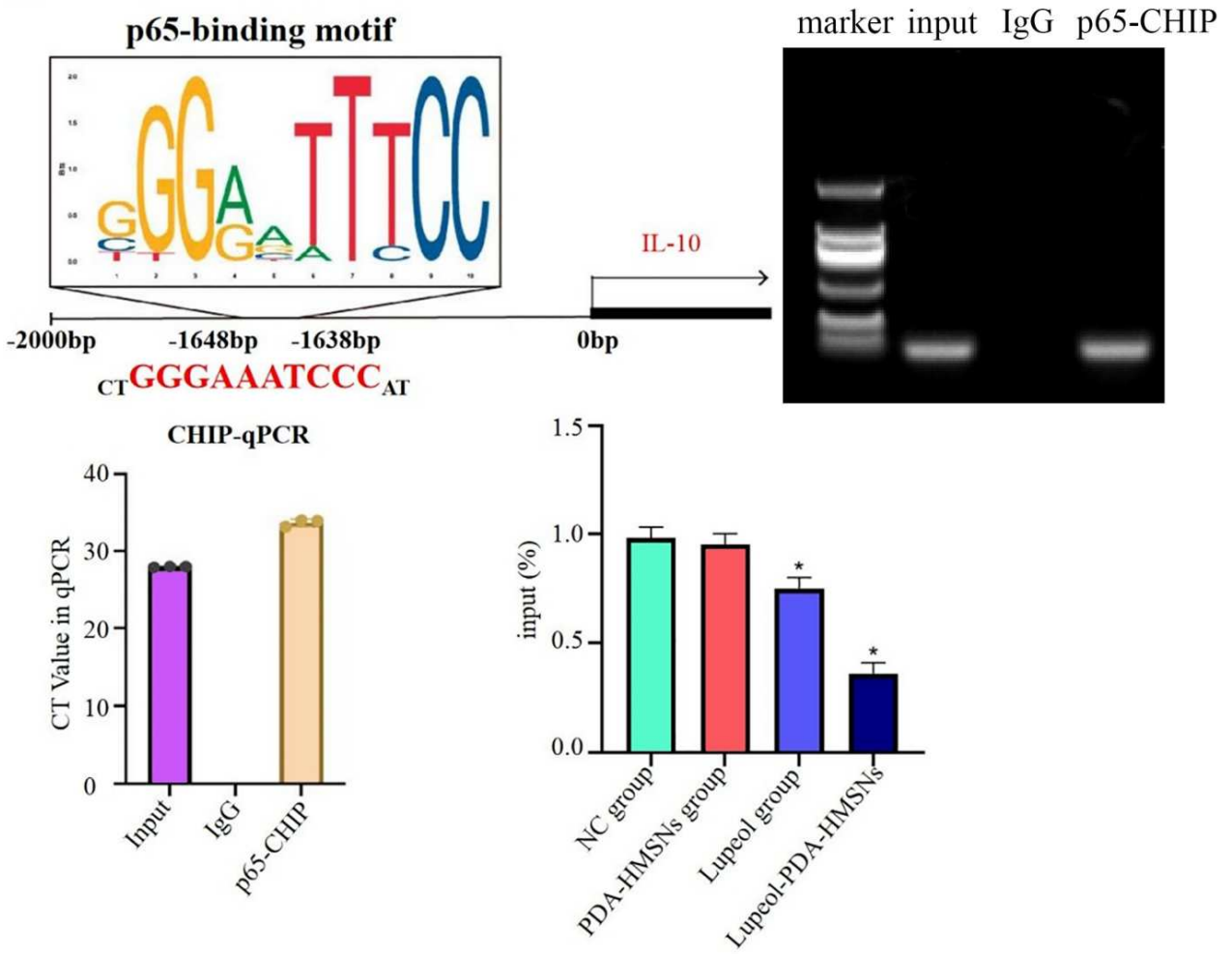

Fig. 6: ChIP-qPCR experiments confirmed that Lupeol-PDA-HMSNs inhibit the binding of NF-κB p65 to the IL-10 promoter and suppress IL-10 transcription (*P<0.05).

DISCUSSION

Lupeol, a natural plant-derived compound primarily found in plants such as Sophora flavescens, exhibits anti-inflammatory, antibacterial, antioxidant and antitumor properties. Studies have indicated that lupeol can downregulate the expression of NF-κB p65, IL-6, IL-10 and TNF-α by inhibiting the NF-κB signaling pathway, thereby modulating the immune microenvironment and suppressing inflammation (Zhou *et al*., 2022). Additionally, lupeol has been shown to upregulate miR-100-5p, consequently inhibiting NCI-H1299 cells in non-small cell lung cancer (Torres-Sanchez *et al*., 2024). These studies indicate that lupeol plays a positive role in cancer treatment. However, its application is limited by low bioavailability and poor targeting. To address these shortcomings, this study innovatively utilized polydopamine-coated hollow mesoporous silica nanoparticles as a carrier and successfully prepared lupeol-loaded nanoparticles. Nevertheless, the mechanism by which lupeol-loaded polydopamine-coated hollow mesoporous silica nanoparticles modulate the immune microenvironment in gastric cancer remains unclear (Fabián *et al*., 2023). Therefore, novel drug delivery strategies for gastric cancer are urgently needed. In this study, by establishing a mouse model, we investigated whether lupeol-loaded polydopamine-coated hollow mesoporous silica nanoparticles could regulate the immune microenvironment in gastric cancer mice by downregulating IL-10 through modulation of the NF-κB signaling pathway.

IL-10, an immunoregulatory cytokine, can weaken Th1-type cellular immune responses by inhibiting the JAK-STAT signaling pathway, thereby reducing inflammation and immune responses within the tumor microenvironment (Traboulsi *et al*., 2025, Shichijo and Yasunaga, 2025). Notably, the expression of IL-10 is transcriptionally regulated by NF-κB. The ChIP-qPCR results from this study further confirm that NF-κB p65 can directly bind to

the IL-10 promoter region and promote its transcription. Therefore, IL-10 can act as a downstream effector of NF-κB, participating in mediating tumor immune escape. Furthermore, upregulated IL-10 can inhibit NF-κB signaling and immune cell activation, thereby weakening their attack on tumor cells and further mediate immune escape. In addition, IL-10 can inhibit the JAK-STAT pathway, suppressing the Th1 cell immune response and consequently reducing inflammation and immune response. Regarding the role of IL-10 in lung cancer, the β subunit of its receptor cooperates with IL-10R1 and the presence of IL-10R2 enhances the binding affinity and signal transduction of IL-10 (Zheng *et al*., 2024, Kim *et al*., 2025). The interaction between the two activates the downstream JAK-STAT signaling pathway. Activated JAK1 and Tyk2 phosphorylate tyrosine residues on the receptor, creating docking sites for STAT proteins. Subsequently, phosphorylated STAT proteins undergo conformational changes, form dimers, translocate into the nucleus, bind to specific gene promoter regions and affect target gene transcription, thereby influencing lung cancer progression. To further explore the mechanism of Lupeol-PDA-HMSNs in gastric cancer, we established a mouse model and found that lupeol exhibits inhibitory effects on gastric tumors (Sen *et al*., 2024). In this study, we found that the Lupeol-PDA-HMSNs exerted prominent inhibition.. Further qRT-PCR results demonstrated high IL-10 expression in gastric cancer cells. Lupeol reduced IL-10 expression and this reduction was more pronounced following Lupeol-PDA-HMSNs intervention.

Abnormally activated NF-κB can promote inflammatory factor production and the inflammatory microenvironment is related to cancer progression (Chen *et al*., 2023). It can also inhibit apoptosis (programmed cell death) to cause tumor cell death (Chen *et al*., 2025). Survival and resistance to treatment (Liang *et al*., 2023). Furthermore, NF-κB activation has been linked to resistance to cancer therapy. To elucidate the mechanism by which Lupeol-PDA-HMSNs regulate the immune microenvironment in gastric cancer, we employed NF-κB inhibitors and activators for comparative intervention. The results of immune indicators demonstrated that after inhibiting NF-κB signaling, the immune microenvironment in the PDTC group was more favorable than that in the Echinulin group. This suggests that NF-κB may play a negative regulatory role in the gastric cancer immune microenvironment. In its activated state, the NF-κB inhibitor IκBα is degraded, leading to the release and nuclear translocation of NF-κB. Lupeol inhibits the ubiquitination and degradation of IκBα, thereby preventing NF-κB activation and suppressing inflammation and NF-κB-related gene expression (Shen *et al*., 2025, Fontana *et al*., 2022). IKK (IκB kinase) is involved in the phosphorylation, ubiquitination and degradation of IκBα. Lupeol can block IκBα degradation by reducing IKK activity; it can also inhibit COX-2 to effectively reduce PGE2 production, ultimately ameliorating inflammation. Furthermore, lupeol can inhibit cytokines such as IL-1, IL-6 and TNF-α, which are capable of activating the NF-κB pathway.

Oxidative stress has been shown to activate the NF-κB signaling pathway. As an antioxidant, lupeol can indirectly suppress NF-κB activation by alleviating cellular oxidative stress (Singha *et al*., 2025, Alam *et al*., 2023). Under Lupeol-PDA-HMSNs intervention, the immune microenvironment exhibited a more favorable trend. During this process, IL-10 is also affected accordingly. Our ChIP-qPCR experiments confirmed that in MFC gastric cancer cells, the NF-κB p65 subunit exhibited significant enrichment at the IL-10 promoter region (-1648 to -1638), indicating direct binding of NF-κB p65 to the IL-10 promoter under physiological conditions. Moreover, compared to the control, PDA-HMSNs and lupeol groups, treatment with Lupeol-PDA-HMSNs significantly reduced p65 enrichment at the IL-10 promoter region. These results demonstrate that Lupeol-PDA-HMSNs can effectively inhibit the binding of NF-κB p65 to the IL-10 promoter, thereby downregulating IL-10 expression at the transcriptional level.

Mechanistically, in MFC gastric cancer cells, NF-κB p65 binds to a specific region of the IL-10 promoter and directly activates its transcription, enabling IL-10 to exert its immunosuppressive function (Dwivedi *et al*., 2026). Lupeol, in its nanoformulation, blocks IKK kinase activity, prevents IκBα degradation and consequently anchors NF-κB p65 in the cytoplasm, inhibiting its nuclear translocation and DNA binding. Simultaneously, it interferes with key modifications such as p65 phosphorylation, attenuating its transcriptional activity. As a result, the binding and activation of the IL-10 promoter by NF-κB p65 are effectively suppressed, leading to significant downregulation of IL-10 expression at the transcriptional level. This alleviates immunosuppression in the tumor microenvironment and offers a potential strategy for combined immunotherapy (Malik *et al*., 2021). Therefore, this study demonstrates that Lupeol-PDA-HMSNs can downregulate IL-10 expression by inhibiting the NF-κB signaling pathway, thereby modulating the immune microenvironment in gastric cancer and promoting tumor cell apoptosis. These findings reveal the crucial role of IL-10 as a downstream target of NF-κB in gastric cancer immune escape and provide experimental evidence for nanoparticle carrier-based immunotherapy in gastric cancer (Zhao *et al*., 2025).

CONCLUSION

Based on the findings above, polydopamine-coated hollow mesoporous silica nanoparticles loaded with lupeol serve as an effective drug delivery system that maximizes therapeutic efficacy and enhances treatment outcomes. This system modulates NF-κB activity and reduces IL-10 expression levels, thereby providing a robust theoretical

foundation for suppressing gastric cancer progression. Nevertheless, this study has several limitations: while animal models have preliminarily validated the efficacy of Lupeol-PDA-HMSNs, their long-term safety, targeting efficiency and immunoregulatory mechanisms in more complex immune microenvironments that better mimic human physiology warrant further investigation. Future studies could employ humanized mouse models or preclinical large-animal experiments to evaluate the translational potential of this approach more systematically.

Acknowledgments
Not applicable.

Funding
This study was supported by Construction Project of Inheritance Studio of Shu Jin, a Distinguished TCM Doctor of Gansu Province (Project No.: 250028).

Data availability statement
The datasets generated and/or analyzed during the current study are available from the corresponding author upon reasonable request.

Authors' contributions
HZ: Proposed the research concept, designed the experimental methodology, conducted the experimental research and drafted the initial manuscript; JG: Performed data organization and analysis, visualized the results and participated in manuscript revision and editing; JS: Conducted experimental validation, provided research resources and contributed to project management and coordination; XW: Corresponding Author: Oversaw the overall research design, provided guidance and supervision throughout the study, secured funding, conducted the final revision and approval of the manuscript and managed the project.
All authors have read and approved the final manuscript.

Ethical approval
This study was approved by the ethics committee of Gansu Provincial Hospital of Traditional Chinese Medicine (NO. 250028). This study was performed in adherence with the ARRIVE guidelines. See supplementary file for the ARRIVE checklist.

Conflicts of interest
The authors declare no conflict of interest.

Supplementary data
https://www.pjps.pk/uploads/2026/05/SUP1778147111.pdf

REFERENCES

Ahmad R, Khan A, Rehman IU, Lee HJ, Khan I and Kim MO (2022). Lupeol treatment attenuates activation of glial cells and oxidative-stress-mediated neuropathology in mouse model of traumatic brain injury. *Int J Mol Sci*., **23**(11): 6086.

Alam F, Kharya AK, Srivastav RK, Akhtar J, Khan MI and Ahmad M (2023). Synergetic effect of lupeol and naringin against bile duct ligation induced cardiac injury in rats via modulating nitrite level (eNos) and NF-kB /p65 expression. *Drug Res (Stuttg)*., **73**(1): 23-29.

Chen B, Liu X, Yu P, Xie F, Kwan JSH, Chan WN, Fang C, Zhang J, Cheung AHK, Chow C, Leung GWM, Leung KT, Shi S, Zhang B, Wang S, Xu D, Fu K, Wong C C, Wu WKK, Chan MWY and Kang W (2023). H. pylori-induced NF-κB-PIEZO1-YAP1-CTGF axis drives gastric cancer progression and cancer-associated fibroblast-mediated tumour microenvironment remodelling. *Clin Transl Med*., **13**(11): e1481.

Chen G and Xie Y (2018). miR-495 inhibits proliferation, migration, and invasion and induces apoptosis via inhibiting PBX3 in melanoma cells. *Onco Targets Ther*., **11**:1909-1920.

Chen Q, Xu Y, Wang Y, Zheng S, Yao T, Qiu J, Qin H and Liang T (2025). Bacteria and tumor debris induced pancreatic cancer progression via the NF-κB signaling pathway. *Cancer Lett*., **632**: 217964.

Chen W, Du J, Li X, Zhi Z and Jiang S (2020). microRNA-137 downregulates MCL1 in ovarian cancer cells and mediates cisplatin-induced apoptosis. *Pharmacogenomics*., **21**(3):195-207.

Dwivedi S, Saini S, - A, Np AK, Bansal A, Sharma RS, Shekhar S, - D, Goel A and Khattri S (2026). NF-κB (p65, p50), IL-18 and IL-10 as therapeutic targets in prostate cancer and BPH: Molecular insights into inflammation-driven pathogenesis. *Asian Pac J Cancer Prev*., **27**(1): 381-388.

Fabian RF, Mayra HM, Manuel ZV, Guadalupe SS, Alejandro PL and Alberto SJ (2023). Characterization of functionalized PLGA nanoparticles loaded with mangiferin and lupeol and their effect on BEAS-2B and HepG2 cell lines. *Anticancer Agents Med Chem*., **23**(10): 1174-1183.

Fontana G, Badalamenti N, Bruno M, Castiglione D, Notarbartolo M, Poma P, Spinella A, Tutone M and Labbozzetta M (2022). Synthesis, *in-vitro* and in-silico analysis of new oleanolic acid and lupeol derivatives against leukemia cell lines: Involvement of the NF-κB pathway. *Int J Mol Sci*., **23**(12): 6594.

Jadidi A, Shokrgozar MA, Sardari S and Maadani AM (2022). Gefitinib-loaded polydopamine-coated hollow mesoporous silica nanoparticle for gastric cancer application. *Int J Pharm*., **629**: 122342.

Kim SH, White Z, Gainullina A, Kang S, Kim J, Dominguez JR, Choi Y, Cabrera I, Plaster M, Takahama M, Czepielewski RS, Yeom J, Gunzer M, Hay N, David O, Chevrier N, Sano T and Kim KW (2025). IL-10 sensing by lung interstitial macrophages prevents bacterial dysbiosis-driven pulmonary inflammation and maintains immune homeostasis. *Immunity.*, **58**(5): 1306-1326.e7.

Kumagai S, Koyama S, Itahashi K, Tanegashima T, Lin YT, Togashi Y, Kamada T, Irie T, Okumura G, Kono H, Ito D, Fujii R, Watanabe S, Sai A, Fukuoka S, Sugiyama E, Watanabe G, Owari T, Nishinakamura H, Sugiyama D and Nishikawa H (2022). Lactic acid promotes PD-1 expression in regulatory T cells in highly glycolytic tumor microenvironments. *Cancer Cell*., **40**(2): 201–218.e9.

Liang Y, Wang Y, Zhang Y, Ye F, Luo D, Li Y, Jin Y, Han D, Wang Z, Chen B, Zhao W, Wang L, Chen X, Ma T, Kong X and Yang Q (2023). HSPB1 facilitates chemoresistance through inhibiting ferroptotic cancer cell death and regulating NF-κB signaling pathway in breast cancer. *Cell Death Dis*., **14**(7): 434.

Livak KJ and Schmittgen TD (2001). Analysis of relative gene expression data using real-time quantitative PCR and the 2(-Delta Delta C(T)) Method. *Methods*., **25**(4):402-408.

Malik A, Naz A, Ahmad S, Hafeez M, Awan FM, Jafar TH, Zahid A, Ikram A, Rauff B and Hassan M (2021). Inhibitory potential of phytochemicals on interleukin-6-mediated T-cell reduction in COVID-19 patients: A computational approach. *Bioinform Biol Insights*., **15**: 11779322211021430.

Mao X, Xu J, Wang W, Liang C, Hua J, Liu J, Zhang B, Meng Q, Yu X and Shi S (2021). Crosstalk between cancer-associated fibroblasts and immune cells in the tumor microenvironment: New findings and future perspectives. *Mol Cancer*., **20**(1): 131

Park JH and Lee DG (2025). Nitric oxide initiates oxidative independent apoptosis-like death in Candida albicans by lupeol. *Biochimie*., **235**: 29-38.

Sen K, Kumar Das S, Ghosh N, Sinha K and Sil PC (2024). Lupeol: A dietary and medicinal triterpene with therapeutic potential. *Biochem Pharmacol*., **229**: 116545.

Shen Y, Jiang K, Tan D, Zhu M, Qiu Y, Huang P, Zou W, Deng J, Wang Z, Xiong Y and Hong D (2025). uN2CpolyG-mediated p65 nuclear sequestration suppresses the NF-κB-NLRP3 pathway in neuronal intranuclear inclusion disease. *Cell Commun Signal*., **23**(1): 68.

Shichijo T and Yasunaga JI (2025). Human T-cell leukemia virus type I: Modulation of viral gene expression and perturbation of host signaling pathways lead to persistent infection. *Curr Opin Virol*., **73**: 101480.

Shiri AM, Zhang T, Bedke T, Zazara DE, Zhao L, Lücke J, Sabihi M, Fazio A, Zhang S, Tauriello DVF, Batlle E, Steglich B, Kempski J, Agalioti T, Nawrocki M, Xu Y, Riecken K, Liebold I, Brockmann L, Konczalla L and Huber S (2024). IL-10 dampens antitumor immunity and promotes liver metastasis via PD-L1 induction. *J Hepatol*., **80**(4): 634–644.

Singha A, Chakraborty A and Sil SK (2025). Lupeol: ethnopharmacological insights and therapeutic potential in human health. *3 Biotech*., **15**(7): 199.

Torres-Sanchez A, Torres G, Estrada S, Perez D, Garcia C, Milian M, Velazquez E, Molina V and Delgado Y (2024). Unraveling the impact of six pentacyclic triterpenes regulating metabolic pathways on lung carcinoma cells. *Pharmaceuticals (Basel)*., **17**(6): 694.

Traboulsi H, Heimbach NS, Wilson ET, Eidelman DH and Baglole CJ (2025). The aryl hydrocarbon receptor promotes the resolution of pulmonary neutrophilia via regulation of macrophage efferocytosis. *J Immunol*., **1950**: vkaf280.

Xu R, Ma L, Chen T and Wang J (2022). Sophorolipid suppresses LPS-induced inflammation in RAW264.7 cells through the NF-κB signaling pathway. *Molecules*., **27**(15): 5037.

Yan S, Zhang C, Ji X, Wu G, Huang X, Zhang Y and Zhang Y (2022). MSC-ACE2 ameliorates streptococcus uberis-induced inflammatory injury in mammary epithelial cells by upregulating the IL-10/STAT3/SOCS3 pathway. *Front Immunol*., **13**: 870780.

Yu Z, Zhang Q, Wei S, Zhang Y, Zhou T, Zhang Q, Shi R, Zinovkin D, Pranjol ZI, Zhang J and Wang H (2024). CD146+CAFs promote progression of endometrial cancer by inducing angiogenesis and vasculogenic mimicry via IL-10/JAK1/STAT3 pathway. *Cell Commun Signal*., **22**(1): 170.

Zhou JC, Wu B, Zhang JJ and Zhang W (2022). Lupeol triggers oxidative stress, ferroptosis, apoptosis and restrains inflammation in nasopharyngeal carcinoma via AMPK/NF-κB pathway. *Immunopharmacol Immunotoxicol*., **44**(4): 621-631.

Zheng G, Ye H, Bai J and Zhang X (2024). Downregulation of lncRNA MIR17HG reduced tumorigenicity and Treg-mediated immune escape of non-small-cell lung cancer cells through targeting the miR-17-5p/RUNX3 axis. *J Biochem Mol Toxicol*., **38**(5): e23715.

Zhao Z, Sun H, Liu Y, Zhang Y, Wang X, Wang X, Tan C, Ni S, Weng W, Zhang M, Wang L, Huang D, Gu W, Chang J, Sheng W and Xu MD (2025). PDPN+ cancer-associated fibroblasts enhance gastric cancer angiogenesis via AKT/NF-κB activation and the CCL2-ACKR1 axis. *MedComm*., **6**(1): e70037.